This full text paper was peer-reviewed at the direction of IEEE Instrumentation and Measurement Society prior to the acceptance and publication
.

Smart ballistocardiography front-end

Guillaume Cathelain
Department of Life Sciences
Ecole Pratique des Hautes Etudes - PSL
Paris, France
guillaume.cathelain@ephe.psl.eu

Bertrand Rivet
GIPSA-Lab
Grenoble INP
Grenoble, France
bertrand.rivet@gipsa-lab.fr

Sophie Achard
GIPSA-Lab
Grenoble INP
Grenoble, France
sophie.achard@gipsa-lab.fr

Jean Bergounioux
Pediatric Intensive Care Unit
Assistance Publique des Hôpitaux de Paris
Garches, France
jean.bergounioux@aphp.fr

François Jouen
Department of Life Sciences
Ecole Pratique des Hautes Etudes - PSL
Paris, France
francois.jouen@ephe.psl.eu

***Abstract*—Ballistocardiography (BCG), a contactless heart rate monitoring method, has the potential to measure vital signs and reduce neonates' monitoring pain and discomfort. It uses an accelerometer on the mattress side. As the signal amplitude is very low, the front-end circuit needs a high amplifier gain and thus is very sensitive to baseline wander and noise. However, the usual analogue baseline wander filters are slow to settle, and the individual plus the bed are a damping system which generates noise at its resonance frequency. Consequently, the BCG signal is likely to saturate for several seconds every time the individual moves. This paper introduces a novel smart BCG front-end which identifies the system resonance frequency, filters the baseline wander and the damping noise, and highly amplifies the BCG signal without saturation after patient movement. It has been successfully tested on an experimental model and opens possibilities for medical, real-time and low-cost applications.**

Keywords—Ballistocardiography, mixed-signal feedback, adaptive noise cancellation, AC coupling, sensor interface

I. Introduction

Ballistocardiography is a non-intrusive monitoring method for cardiac activity. It was invented at the end of the 19th century but supplanted by the first electrocardiographs, improving precision and robustness at that time. Today, with new sensor technologies and digital signal processing, this technology is gaining renewed interest. Ballistocardiography's principle relies on measuring ballistic forces [1]: during ventricular systole, blood is ejected from the left ventricle through the aortic arch, generating a pulsed cardiac ballistic force that slightly strains the bedding and the bed frame on which the patient is lying or sitting. This mechanical phenomenon allows cardiac monitoring through contactless measurements of a pressure variation (e.g strain gauge) or a deformation (e.g accelerometers) of the patient bed or mattress. A ballistocardiogram (BCG) is a record of this mechanical phenomenon (Figure 1).

Due to the mechanical focus of the sensors, respiratory and motor activities are often recorded along the ballistocardiogram, which gives valuable information on the overall physiological state of the individual.

This monitoring technology has many applications in the medical field. As it is contactless and low-cost, it is adapted for long term and home surveillance of cardiovascular diseases. Heart failure and sleep apnea may be prevented in geriatrics [2,3]. For children in hospital, the physiological state (cardiac and respiratory activities) is usually evaluated by electrocardiography (ECG) and photoplethysmography (PPG). The former uses electrodes on the thorax and on the limb's extremities; the latter uses pulse oximetry probes that tweak either a finger or a toe. Monitoring children is difficult because of their high spontaneous mobility that leads to repetitive artifacts and false alarms. Moreover, electrodes peel off the epidermis and pulse oximetry probes can regularly detach from the finger or toe. Several factors are involved: the child twitches and pulls the probes, the electrode adhesive is worn or the nursing staff could not properly set up the electrodes. Children pain, which may be monitored by heart rate variability [4] or infrared thermography [5], affects the neuro-motor and cognitive development especially for preterm neonates [6]. Finally, the actual equipment is expensive to install and maintain; it must be changed or replaced several times during hospitalization and frequently in the same day. Consequently, a non-intrusive apparatus would represent a major progress to detect children heartbeats in a harmless way.

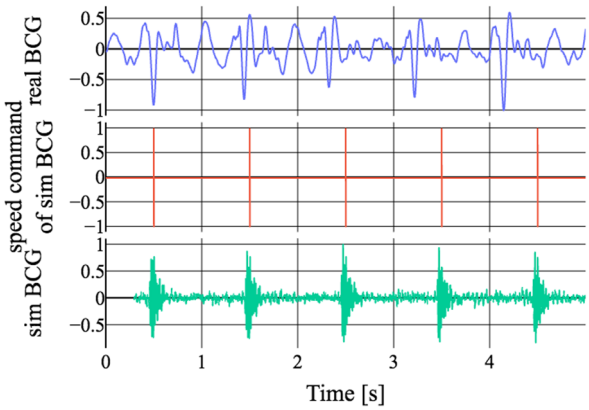

Figure 1: A typical BCG compared to the simulated cardiac force. Signals' amplitudes have been normalized by zero-mean and one-maximal amplitude.

Digital signal processing algorithms have been developed to detect heartbeats, beat-to-beat heart rate and heart rate variability in BCG signals using time domain or time-

978-1-7281-4460-3/20/$31.00 ©2020 IEEE

frequency domain methods [7]. Noise robustness has also been investigated and specific heartbeat detection algorithm [8] have been designed in the case of pediatric BCG, whose amplitude, compared to adults, can be about 30 times lower due to low weight and low cardiac contractile force [9].

Analog amplification is also required to achieve good detection performance. Therefore, it is very sensitive to baseline wander that occurs at a position shift, e.g. from supine to prone position, and needs to be filtered. However, in order to measure the respiratory activity whose lowest frequency components are about 0.1 Hz [10], the usual high-pass filters are slow to settle and the BCG signal can saturate for several decades of seconds as it will be shown in this paper. The addition of non-linear components, e.g. commutation diodes in the amplifier feedback loop [11], may help reduce the amplifier settling time, i.e. the time before the end of the saturation, for a few seconds only. Moreover, the individual plus its bed may be considered as a damping system which generates noise at its resonance frequency. Environmental noises, e.g. nurses walking, ventilation apparatus or during transportation in pediatric intensive care unit, can also occur. For the same saturation reasons, these repetitive noises need to be filtered otherwise the monitoring coverage might be lowered.

In this context, this paper introduces a novel smart BCG front-end which identifies the system resonance frequency, filters the baseline wander and the damping noise, and highly amplifies the BCG signal without saturation after movement. The remaining of this paper is organized as follows: Section 2 presents the materials and Section 3 details the proposed method before results in Section 4. Finally, Section 5 concludes this study.

II. Materials

A reduced experimental model was designed to demonstrate the amplification and filtering principle of the smart BCG front end in a controlled environment.

A. Experimental model

The experiment uses a spring-mass model of a baby body lying on a bed, as illustrated on Figure 2.

Figure 2: Body lying on a bed at left and reduced model at right

Firstly, the bed is taken from the intensive care unit (Villard reference 505.59). It is made of steel and the security bars were up during the experiment.

Secondly, the Pharmaouest polyurethane mattress dimensions are 120x60x10 cm (length x width x height).

Thirdly, the weight, representing the thorax, is a steel, 10cm-wide diameter and 3.4 kg cylinder. The typical average pressure of a thorax lying on a mattress is set at 32 mmHg, which is near the typical 20 - 40 mmHg intracapillary pressure range [12]. The weight's material is a high-density steel. In order to apply the thorax typical pressure on the spacer fabrics layer, its diameter could not respect the ratio of the reduced model because the cylinder would have been too long and thus unstable.

B. Cardiac force and noise simulation

Considering the experimental model, the simulated cardiac force should have the characteristics of a BCG. In order to simplify the model, the cardiac force is simulated by a series of sinusoidal pulses, repeated every second. The average BCG pulse is in the 5 to 10 Hz frequency range and approximately lasts 160 ms and has an approximate 1 N amplitude [1].

To our knowledge, no commercially and compact device can generate such a vibration, consequently it was decided to simulate the cardiac force using a MakeBlock 42BYG stepper motor. It has been previously unbalanced by fixing a 36 g and 3 cm eccentric steel screw on the rotor, as seen in Figure 2. The centrifugal force equals 1.2 N at 300 rpm or 5 Hz; it can be adjusted to different speed by updating the weight and position of the eccentric. The stepper motor was initially programmed to generate an average BCG waveform, i.e. pulsed vibrations, by rotating at 300 - 600 rpm during 160 ms every second. However, the stepper motor acceleration is too fast and is stepped at low speed, which generates shocks and noises when the vibration starts and ends. Finally, for practical reasons, the BCG was simulated using the acceleration shocks when the rotor starts rotating. The speed command profile is illustrated at Figure 1. The impulse response of the bed, acting like a damping system, generates noises at the resonance frequency. The simulated vibration differs in frequency range from the average BCG, and the amplitude have not been investigated. Nevertheless, the demonstration of the underlying principle remains the same.

In parallel, vibrations at different constant frequencies were generated to accurately measure the frequency response of the amplifier.

C. Electronics components

For measuring the simulated BCG signal, several sensors and electronics components are used. They are listed below and integrated in an ABS enclosure, referenced as 1591XXTGY by Hammond Manufacturing.

The digital signal processor (DSP) is a 32-bit STM32L476, mounted on a Nucleo-L476RG board, whose analog-to-digital converters (ADC) and digital-to-analog converters (DAC) channels have a 12 bits resolution and a 256 Hz sampling rate. The ARM MBED operating system was used with CMSIS DSP library. A USB port is used for serial communication with a computer and powering up the circuit.

The sensor is a LIS344ALH accelerometer with a 50 $\mu g/\sqrt{Hz}$ low noise density and a 0.66 V/g high sensitivity. It is mounted on a STEVAL-MKI015V1 evaluation board, and the FS, PD and ST pins are grounded. It is powered by a 3.3 V single supply and measures $\pm 2\ g$ accelerations in this configuration. It is oriented such that the Z-axis is in the gravity direction.

The amplifier used is an AD623AN instrumentation amplifier whose gain is adjustable thanks to a resistor and ranges from 0 to 40 decibels (dB). Its voltage reference $Vref$ equals half the accelerometer voltage supply.

III. Methods

In this section, the mixed signal front-end architecture is detailed, as well as the digital filters used for baseline wander removal. Lastly, the noise frequency identification and filtering algorithm is explained.

A. Mixed signal front-end

A mixed signal architecture is a topology where an analogue signal is digitized by an ADC, filtered on a DSP then synthesized by a DAC [13]. Such circuits have the same advantages as numerical filters, e.g. sharp transition frequency band or fast settling time, and may be associated with an analogue amplifier.

In the BCG case, undesired components of the analogue acceleration signal have to be filtered before amplification and digitization. The designed architecture, illustrated at Figure 3, removes those undesired components and amplify the resulting signal using an instrumentation amplifier.

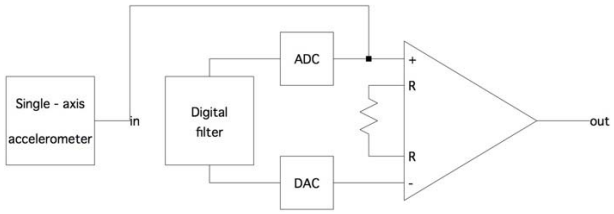

Figure 3: Pseudo electronic circuit of the front-end

The resulting signal is expressed by (1), where G stands for the gain of the amplifier and f stands for the digital filter.

$$V_{out} = G\,.[Vin - f(Vin)] \tag{1}$$

Similar architectures have been used in biosignal processing. In 2003, AnalogDevice proposed an electrocardiography front-end using the ADuC842 microcontroller with a simple stepwise feedback on the AD620 instrumentation amplifier's reference offset pin [14]. In 2004 and more recently, electroencephalography front-end have integrated highpass filters for baseline wander removal [15, 16]. However, these papers only focused on baseline wander removal, with a cut-off frequency much less constraining than in the BCG case (5 and 0.05Hz for EEG and BCG respectively).

While synthesizing the feedback signal, a saturation is implemented in order to respect (2).

$$0 < G.[Vin - f(Vin)] + Vref < 3.3 \tag{2}$$

B. Digital filters design and implementation

In order to remove the undesired signal components, two types of digital linear filters have been investigated: finite impulse response (FIR); and cascade of second order infinite impulse response (IIR) filters, defined at Figure 4 and commonly known as cascade of biquad filters. FIR and biquad filters are respectively defined by (3) and (4), where n is the sample index, x and y are the input and output signals, N is the number of coefficient, $\{a_n\}$ and $\{b_n\}$ are the feedback and feedforward coefficients.

$$y[n] = b_0.x[n] + \cdots + b_{N-1}.x[n-N+1] \tag{3}$$

$$y[n] = b_0.x[n] + b_1.x[n-1] + b_2.x[n-2] + a_1.y[n-1] + a_2.y[n-2] \tag{4}$$

By convention, a_0 is set to 1.

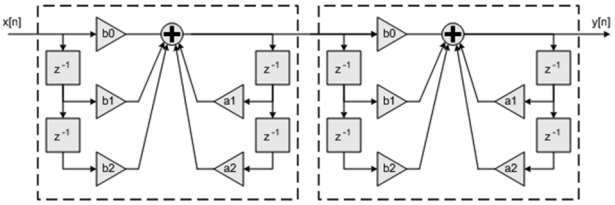

Figure 4: Example of a 4th order IIR filter, cascade of two biquad filters, as implemented by the CMSIS DSP library.

Filter coefficients are computed using the scipy.signal Python library on a 64-bits computer. They have to be quantified to 32-bits coefficients before being implemented on the DSP, which may generate errors especially for IIR filters with high constraint filters and very low cut-off frequency. For example, Figure 5 illustrates the quantization of poles for a second order Butterworth filter with 0.05 Hz cut-off frequency and 256 Hz sampling rate.

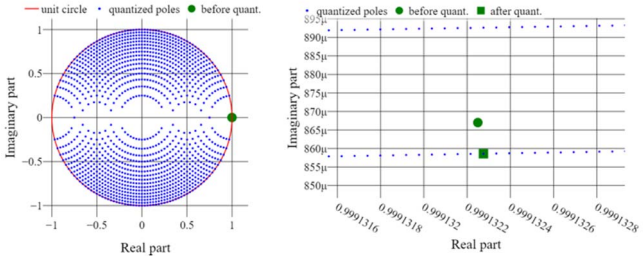

Figure 5: 6 bits poles distribution at left; 64 bits to 32 bits quantization of a pole at right.

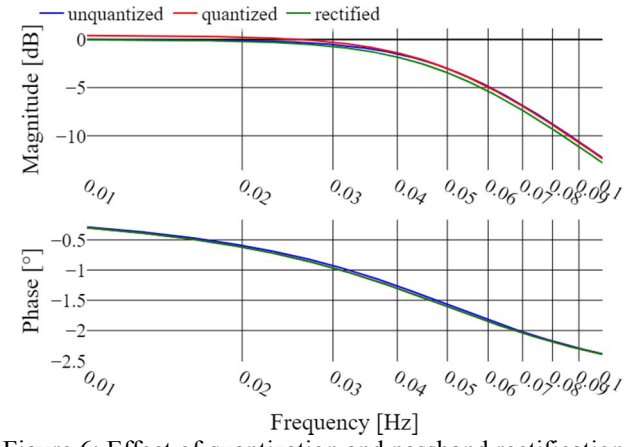

Figure 6: Effect of quantization and passband rectification.

This coefficient quantization is likely to modify the frequency response of the filter, e.g. the bandpass gain as illustrated in Figure 6 using the same filter as in Figure 5.

After quantization, the bandpass gain was systematically corrected to 0 dB using (5).

$$b'_n = b_n \frac{\sum a_i}{\sum b_j} \quad (5)$$

The settling time of the filters depends on initialization. The state of the filter is usually initialized to zero: the signal is thus causal. However, the sensor has a rest position that is known or can be estimated. It may be assumed that the accelerometer is laid flat on the mattress which is itself horizontal: the z axis should see approximately a +1 g offset value, so 2.31 V in this setting. The filter is initialized considering that the signal is 2.31 V before starting the record.

C. *Baseline wander removal*

A commonly undesired component of physiological signal is the baseline wander. It is a low frequency component that prevents a high gain amplification. In ballistocardiography, the baseline wander is a voltage offset depending on the body position and weight in the bed. For example, during a patient position shift, the accelerometer orientation and the gravity projection on the accelerometer axes change. We observed that this offset value ranges typically from 0.1 to 0.5 g, for which the amplifier would saturate with $G > 3\,dB$.

The respiration, whose frequency ranges from 0.5 to 1.0 Hz in neonatology [17] and down to 0.1 Hz in geriatrics [10], can be considered either as a part of the baseline wander or as a useful component of the signal. In this paper, the respiration is not filtered, consequently the cut-off frequency of the baseline wander filter is set at 0.05 Hz and f is a low pass filter defined by (1).

In the FIR case, the window method is applied with a Kaiser window of 40 dB minimal attenuation in the passband and a 0.1 Hz transition bandwidth. The resulting FIR filter has 5716 coefficients.

In the IIR case, a second order Butterworth filter, chosen because of its maximally flat response in the passband, is designed and repeated twice in order to sharpen the transition. In this paper, the selected filter is this fourth order IIR filter, because the FIR filter is too computation-expensive for the microcontroller.

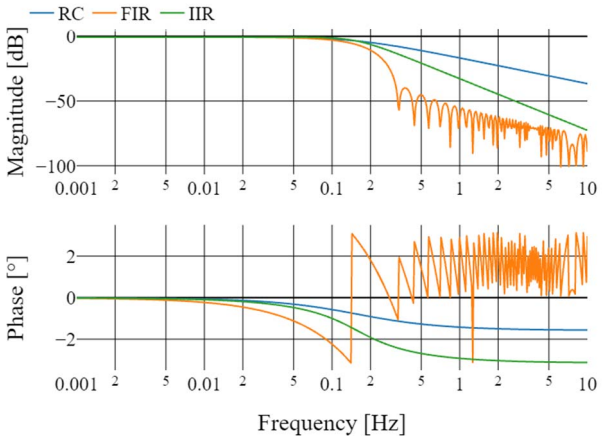

Figure 7: Frequency responses of the lowpass equivalent of the designed filters and the typical analogue RC filter.

The Figure 7 illustrates the responses of the designed FIR and IIR filters low pass equivalent. They are compared to a typical first order resistor-capacitor (RC) filter with the same cut-off frequency.

Furthermore, a gain of 21 dB is set in the experiment. The high-pass equivalent filter finally has the following numerator and denominators in Table 1. It is defined by (6), (7) and (8).

$$V_{out} = g(Vin) \quad (6)$$

$$a'_n = a_n \quad (7)$$

$$b'_n = G.(a_n - b_n) \quad (8)$$

Table 1: Numerators and denominators of the high-pass equivalent filter.

a0	1
a1	-1.9982646
a2	0.99826604
b0	11.183295
b1	-22.3472
b2	11.163904

D. *Noise frequency identification and filtering*

The noise frequency is identified and filtered using the embedded algorithm detailed at Figure 8, where signal stands for amplified signal.

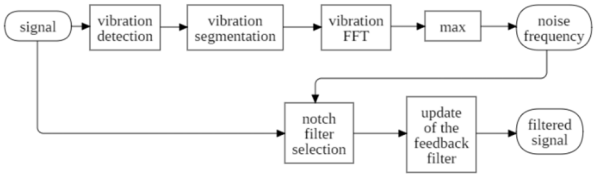

Figure 8: Noise frequency identification and filtering pseudo-algorithm

The vibration detection step is parametrized by a voltage threshold, hereafter referred as $threshold$, over which the vibration is detected. The vibration starts there and has a fixed $duration$.

The power spectral density of the segmented vibration is computed by the microcontroller. Its maximum is located at the noise frequency so that it is outside the BCG frequency range, otherwise the heartbeats in the BCG signal would be distorted or filtered.

Several notch filters, with $Q = 0.707$ quality factors have been previously computed using the scipy.signal library outside the microcontroller. The notch filter whose frequency is the closest to the noise frequency is selected, and added to the IIR baseline wander filter.

IV. Results

In this section the results of the experiment are detailed: the baseline wander filtering, the settling time comparison and the noise identification and filtering. The shown raw signals are not post-processed.

A. *Baseline wander filtering*

The IIR filter succeed in filtering the baseline wander, and it is removed by the amplifier. At steady state, the maximal peak to peak amplitude of the pulses are ten times higher on the output than on the input. Figure 9 is an illustration of the signal before and after the amplifier with pulses amplitude below the noise level.

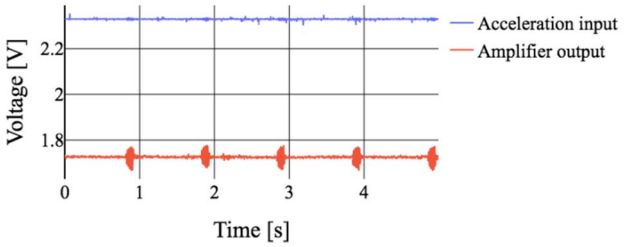

Figure 9: Illustration of baseline wander removal with 21 dB amplification.

Using this filter, vibrations at different constant frequencies are generated and the measured accelerations are compared before and after filtering and amplification by their root-mean-square values. The experimental frequency response is compared to the designed filter at Figure 10.

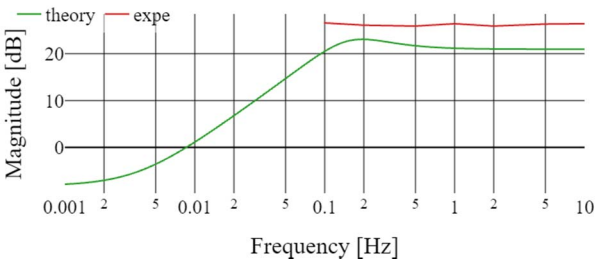

Figure 10: Comparison of frequency responses for a 21 dB gain, quantized IIR versus experimental points

B. *Settling time comparison*

Signals were recorded at different initialization settings. Figure 11 is a superposition of two signals at different times, with 0 V and 2.31 V offset initialization. When the state of the filter is initialized at 0 V, the amplifier can saturate for decades of seconds, which is not the case if the offset is well estimated.

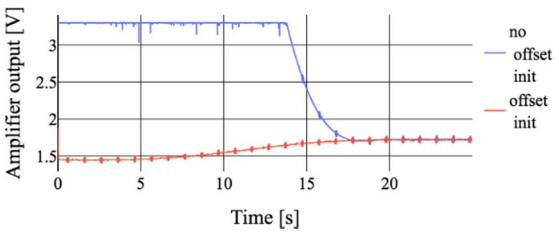

Figure 11: Effect of offset initialization on settling time.

The settling time depends on offset initialization, as illustrated by Figure 12.

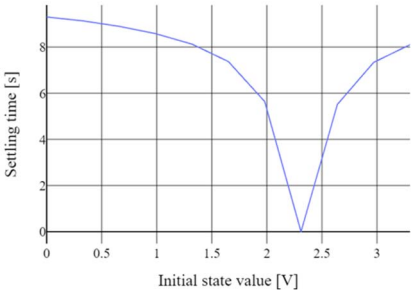

Figure 12: Settling times for different offset initialization with a 21 dB amplification.

C. *Noise identification*

The *threshold* and *duration* were set at 1.5% of the baseline wander and 0.25 s respectively. Noise was generated by pulsed vibration, i.e. the simulated BCG. The noise frequency determined by the microcontroller is approximately 68 Hz, as it can be seen in Figure 13. This is the resonant frequency of the damping system.

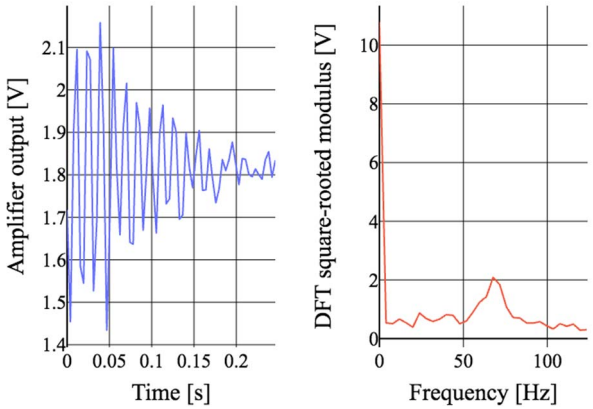

Figure 13 : Example of a simulated BCG pulse and its single-sided frequency spectrum computed by the microcontroller.

A notch filter was then selected by the algorithm illustrated by Figure 8 to filter the identified noise frequency.

V. DISCUSSION

This paper introduced a novel smart BCG front-end which identifies the system resonance frequency, filters the baseline wander and the damping noise, and amplifies the BCG signal without saturation after patient movement.

During the experimentations, a limited 21 dB gain was used for illustrating the principle of the smart BCG front-end. Higher gains resulted in noisy signals and saturation, due to the use of prototyping boards rather than a specific electronics circuit with a proper ground plane. In the future, an amplifier with a higher gain will be designed and tested on real patients.

Compared to usual BCG instrumentations, this conditioning circuit has a lower settling time and a sharper frequency transition.

The principle of a smart BCG front-end has been demonstrated; it opens possibilities for medical, real-time and low-cost applications.

ACKNOWLEDGMENT

The authors would like to thank the reviewers for their help and constructive suggestions.

This work has received support under the program "Investissements d'Avenir" launched by the French Government and implemented by ANR with the references ANR-10-LABX-XXX and ANR-10-IDEX-0001-02 PSL. It is part of a technology co-developed with the Fealing startup company (www.fealing.eu).

REFERENCES

[1] C-S. Kim, S. L. Ober, M. S. McMurtry, B. A. Finegan, O. T. Inan,and R. M. Hahn,"Ballistocardiogram: Mechanism and Potential for Unobtrusive Cardiovascular Health Monitoring", *Nature Scientific Reports*, vol. 6, no. 31297, Aug. 2016.

[2] V. B. Aydemir, J. Fan, S. Dowling, O. T. Inan, J. M. Rehg, and L. Klein, « Ballistocardiography for Ambulatory Detection and Prediction of Heart Failure Decompensation », *Journal of Cardiac Failure*, vol. 24, issue 8, Supplement, pp. S116, Aug. 2018.

[3] Z. Wang, X. Zhou, W. Zhao, F. Liu, H. Ni, and Z. Yu, « Assessing the severity of sleep apnea syndrome based on ballistocardiogram », *PLoS One*, Apr. 2017.

[4] B. M. Appelhans, and L. J. Luecken, "Heart rate variability and pain: Associations of two interrelated homeostatic processes", *Biological Psychology*, vol. 77, no. 2, pp 174-182, Feb. 2008.

[5] S. Brummelte, R. E. Grunau, V. Chau, K. J. Poskitt, R. Brant, J. Vinall, A. Gover, A. R. Synnes, and S. P. Miller, "Procedural pain and brain development in premature newborns," *Annals of Neurology*, vol. 71, no. 3, pp 385-396, Feb. 2012.

[6] A. Alalwani, Y. Chahir, B. Guillois, M. Molina, and F. Jouen, "Neonatal Pain Recognition using LBP descriptor and Wavelet Thresholding Technique", *IEEE International Conference on Multimedia Computing and Systems*, Apr. 2014.

[7] O. T. Inan, P-F. Migeotte, K-S. Park, M. Etemadi, K.Tavakolian, R.Casanella, J.Zanetti, J. Tank, I.Funtova, G. K. Prisk, and M. DiRienzo, "Ballistocardiography and seismocardiography: A review of recent advances", *IEEE Journal of Biomedical and Health Informatics*, vol. 19, no. 4, pp. 1414-1427, Jul. 2015.

[8] G. Cathelain, B. Rivet, S. Achard, J. Bergounioux, and F. Jouen "Dynamic Time Warping for heartbeat detection in ballistocardiography", *2019 Computing in Cardiology Conference*, Dec. 2019.

[9] M. Erkinjuntti, K. Vaahtoranta, J. Alihanka, and P. Kero, "Use of the SCSB method for monitoring of respiration, body movements and ballistocardiogram in infants", *Early Human Development*, vol. 9, pp 119-126, Feb. 1984.

[10] A. Rodríguez□Molinero, L. Narvaiza, J. Ruiz, C. Gálvez□Barrón, "Normal Respiratory Rate and Peripheral Blood Oxygen Saturation in the Elderly Population", *Journal of the American Geriatrics Society*, vol. 61, issue 12, pp. 2238-2240, Dec. 2013.

[11] Texas Instrument, « Fast-settling low-pass filter circuit », *Analog Engineer's Circuit: Amplifiers*, SBOA244, Jan. 2019.

[12] C. Turnage-Carrier, K. M. McLane, M-A. Gregurich, "Interface Pressure Comparison of Healthy Premature Infants With Various Neonatal Bed Surfaces", *Advances in Neonatal Care*, vol. 8, issue 3, pp. 176–184, Jun. 2008.

[13] W. Kester, "Mixed-Signal Design Seminar", *Analog Devices*, 1991.

[14] E. Company-Bosch, E. Hartmann, « ECG Front-End Design is Simplified with MicroConverter® », *Analog Dialogue*, vol. 37, Nov. 2003.

[15] R. Muller, S. Gambini, « A 0.013 mm , 5 W, DC-Coupled Neural Signal Acquisition IC With 0.5 V Supply », *IEEE Journal Of Solid-State Circuits*, vol. 47, no. 1, Jan. 2012.

[16] M. Mojarradi, T. Johnson, M. Ortiz, T. Cunningham, R. Andersen, « Low-Cutoff, High-Pass Digital Filtering of Neural Signals », *NASA Tech Briefs*, pp. 11, Sep. 2004.

[17] S. Reuter, C. Moser, M. Baack, "Respiratory Distress in the Newborn", *Pediatrics in Review*, vol. 35, issue 10, pp. 417–429, Oct. 2014.